CMTC-485740-MS

Performance Evaluation for Carbon Sequestration in Shale Gas Reservoir Systems

Langtao Zhu, China University of Petroleum (Beijing), Xinwei Liao, China University of Petroleum (Beijing), Zhiming Chen, China University of Petroleum (Beijing), Xuyang Cheng, China University of Petroleum (Beijing)

This paper was prepared for presentation at the Carbon Management Technology Conference held in Houston, Texas, USA, 17-20 July 2017.

Abstract

Storage CO_2 in shale formation is considered as a promising option to reduce CO_2 emissions and enhance shale gas recovery. Many simple analytical and semi-analytical techniques have been proposed to support screening analysis and performance assessment for potential carbon sequestration sites. However, these analytical techniques have ignored the effect of fracture occurrences, which are important to the carbon sequestration in shale formation.

In this paper, numerical simulation technology is applied to model different complex hydraulic fracture occurrences and evaluate the CO_2 seepage rule during carbon sequestration. First, multi-component Langmuir isotherm is applied to simulate the adsorption desorption phenomenon of CO_2. Combining Langmuir isotherm with the reservoir parameters of Barnett shale formation, shale reservoir simulation model is constructed to simulate the CO_2 seepage law during the CO_2 sequestration. Then, based on the shale reservoir simulation model, local grid refinement technology is used to characterize the five typical fracture occurrences caused by hydraulic fracturing. Subsequently, the numerical simulation cases with five different fracture occurrences are run to evaluate the performance during CO_2 storage process. Finally, some critical important parameters, including engineering and geologic parameters, are evaluated through the sensitivity study. In order to identify and illustrate the performance which progressively occur over time, the log-log plot of CO_2 injection rate versus time is adopted.

The simulation results indicate that the flow regimes of CO_2 injection can be classified into eight flow regions. Among these flow regions, the inner boundary dominated flow regime is a unique one which can occur only when realizing strongly stimulated reservoir volume. Further, the sensitivity study indicates that the fracture topologies and the primary fracture conductivity are the two key factors dominating the early-time flow behavior during the carbon sequestration. And the final-time flow behavior is dominated by the shale reservoir parameters.

This work systematically analyzes the effect of fracture topologies on carbon sequestration and enlarges our knowledge of CO_2 storage in shale gas systems.

1. Introduction

Shale gas has become an increasingly important source of natural gas (CH_4) in the United States over the last decade. Due to its unconventional characteristics, injecting carbon dioxide (CO_2) to enhance shale gas recovery (CO_2-EGR) is a potentially feasible method to increase gas-yield while realizing CO_2 sequestration (CS). Therefore, it is more and more important to quantitatively demonstrate the influence of various reservoir and completion parameters on performance of multiply-hydraulic fractured horizontal wells (MFHW) in the process of CO_2 injection.

Ultra-tight shale reservoirs present numerous challenges to modeling and understanding. These reservoirs typically require hydraulic fracturing, which will increase the productivity and create complex fracture profiles. Additionally, CO_2 has a much higher sorption affinity to kerogen than CH_4, which will induce strongly multi-component competitive adsorption phenomenon. This phenomenon will remarkably affect the flow event and result in an unintuitive (difficult-to-model) pressure profile

behavior.

According to single-component and multi-component competitive adsorption isotherm based on the Langmuir isotherm, various analytical (Bumb and Mckee, 1988), semi-analytical, and numerical models have been proposed to characterize rate and pressure behavior versus time in shale gas systems featuring horizontal wells with multi-cluster staged hydraulic fractures:

1) Analytical and semi-analytical models. At present, the analytical and semi-analytical models can only describe the adsorption phenomenon of single-component based on the Langmuir isotherm. And the fundamental methods are Stehfest function and the point source method proposed by Ozkan (Brown et al., 2011; Stehfest, 1970). Applying these methods, a lot of analytical and semi-analytical empirical models were proposed to evaluate the production data. In these models, MFHWs with symmetric or asymmetric bi-wing fractures (Fig.4-a) were initiatively proposed to reveal the seepage rule based on the production performance(Liu et al., 2015; Ren and Guo, 2015; Sureshjani and Clarkson, 2015; Wang, 2014). Meanwhile, much fracturing imaging strongly shows that complex fracture networks can easily develop along bi-wing fractures for the natural fractures (Fig.4-d)(Stalgorova, 2012; Stalgorova and Mattar, 2013). With the development of the multiply-hydraulic fracturing technology in recent years, complex fracture networks can easily develop along horizontally fractured well, as shown in Fig. 1&Fig.4-e (Dongyan et al., 2015; Ali et al., 2013; Chen et al., 2015). Although a lot have been achieved in the performance predicts of MFHWs with fracture networks by means of analytical and semi-analytical methods, these methods can't accurately and effectively describe the performance of MFHW for the complexity of fracture network and multi-component competitive adsorption phenomenon.

2) Numerical simulation models. Compared with the analytical and semi-analytical methods, the numerical simulation method is becoming the main method to study the shale gas reservoir because it can model complex fracture networks and simulate multi-component competitive adsorption phenomenons. The local grid refinement method (LGR) is adopted to model the hydraulic fracture to accurately simulate nonlinear flow. Additionally, the extended Langmuir isotherm (EL) is applied to systematically evaluate the potential of CO_2-EGR and CS in the shale reservoir (Ruthven, 1984; Ritter and Yang, 1987). Many scholars adopt numerical simulation method to quantitatively demonstrate the influence of fracture topologies (as shown in Fig.4) on performance of fractured vertical or horizontal wells in tight gas and shale gas reservoir systems (Godec et al., 2013; Bacon et al., 2015; Freeman et al., 2013). And they further study the influence of multiply-hydraulic fracturing (Fig. 1) on performance of MFHW (Jones et al., 2013). Despite a lot of published numerical studies about the effect of fracture topologies, there are few people synthetically study the flow behavior of injecting CO_2 through MFHW.

In this paper, the EL isotherm is modeled to simulate the competitive adsorption phenomenon between CO_2 and CH_4. And we further systematically evaluate the influence of various reservoir and completion parameters on the CO_2 injection procedure:(1) A dual-porosity model is incorporated in the reservoir simulation model. (2) Local grid refinement (LGR) is adopted in the simulation runs to improve the simulation accuracy of hydraulic fractures. (3) Base on the topology of SRV (Fig.1 & Fig.4-e), CO_2 injection rate behavior analysis is conducted to confirm the seepage rule of CO_2 injection in shale gas reservoir systems. (4) Sensitivity analysis is conducted to confirm the effect of various geologic, engineering, and operating parameters on the performance of MFHW.

This work presents a novel perspective on investigating the flow behavior of CO_2 injection in shale gas system.

2. Description of numerical model

To assess the flow event of the CO_2 injection process in shale gas reservoir, a set of numerical simulation studies run to simulate the process of CO_2 injection. Barnett shale is selected as the representative shale gas reservoir and the correlation parameters are presented in Table.1 (seen in Appendices). And a model for multi-component transport in dual-porosity sorbing media is constructed. The following introduces key models describing porosity and permeability evolution in both matrix and fracture networks including the coupling between these two media.

2.1. Field and constitutive equation

Field and constitutive equations for gas flow and transport in shale are defined (Eshkalak et al., 2014). These equations are coupled through porosity and permeability evolution driven by Langmuir sorption. Generally, the multi-component fluid flow of gas in a dual-porosity model is considered in constructing the geologic model of shale gas reservoirs based on a modified Warren and Root's model. In this model, the natural and hydraulic fractures are the flow channel. And the matrix is the main reservoir space. The intercommunication between the inter-granular void spaces is controlled by diffusion law driven by Langmuir sorption. The coupled flow and mass transport processes involving fluid-rock interactions can be written as: (given by Eq.(1)).

$$\begin{aligned}\frac{V}{\Delta t}(N_i^{n+1}-N_i^n) &= \Delta T_g \rho_g y_i \phi(convection)\\ &+ \Delta A D_{ig} \Delta(\rho_g y_{ig})(diffusion+dispersion)\\ &+ q_i(injeciton/\ production)\end{aligned} \tag{1}$$

where N^n denotes the moles per unit of grid block volume at the n moment, V is the grid block volume, Δt is time step, The first term to the right of the equation is the convection term, T is the transmissibility of gas phase, ρ is the molar density of

gas phase, y is the mole fraction in gas phase, ϕ is the porosity. The second term to the right is the diffusion and dispersion term, where A is an empirical correction factor of *D*, *D* is the diffusion and dispersion coefficient. The last term denotes injection or production rate. Subscripts *i* and *g* respectively represent the number of component and the gas phase. The following assumptions apply:

1) The shale reservoir is a homogenous, isotropic and elastic continuum. The system is isothermal.
2) Gas present within the system is ideal.
3) Gas flow through the fractures in shale conforms to Darcy's Law (the water phase is not considered in this study and the original gas component is 100% CH_4). Gas transport in the shale matrix is assumed to obey Fick's Law.
4) Gas sorption only occurs within the matrix.

2.2 Competitive adsorption and desorption between CH_4 and CO_2

Organic matter of shale formation has shown stronger adsorption potential of carbon dioxide (CO_2) compared to methane (CH_4) according to experimental studies. The gas desorption from or adsorption onto kerogenic media has been studied extensively in coal-bed methane reservoirs. However, the sorption, adsorption, and transport properties of shale are not necessarily analogous to coal (Schettler and Parmely, 1991). Currently the commonly used empirical model for single-component surface sorption is the Langmuir isotherm (given by Eq. (1)) and the Freundlich isotherm. For the multi-component competitive adsorption phenomenon, the extended Langmuir isotherm is proposed (given by Eq. (2))(Ruthven, 1984; Ritter and Yang, 1987b).

$$V_{ads,i}(P) = V_{Li}\frac{y_i P}{P_{Li}(1+\sum_{j=1}^{m} y_j \frac{P}{P_{Lj}})}, i = 1,.....,m,..... \quad (2)$$

Where the V_L term represents the total storage at infinite pressure and the pressure at which half of this volume is stored (P_L), V_{ads} is the potential releasable-gas content in scf/ton, *P* is pore pressure (assumed as the average reservoir pressure), y is hydro carbon mole fraction in gas phase, m is the total number of component in gas phase. Subscripts *i* and *j* represent the number of component. Additionally, the extended Langmuir model assumes instantaneous equilibrium of the sorptive surface and the storage in the pore space i.e., there is no transient lag between pressure drop and desorption or adsorption response.

2.3. Permeability model for hydraulic fracture

The multiply-hydraulic fracturing can create complex fracture network which obviously improves the conductivity near horizontal well. In order to improve the simulation accuracy for regions around hydraulic fractures, local grid refinement (LGR) is widely applied to model different fracture occurrences in the simulation runs (Eshkalak et al., 2014b; Yu et al., 2014). The transmissibility of the fracture blocks was adjusted to obey the following relationship (given in Eq.3). In addition, when the fractures intersect, the staggered mesh is equal to the primary fractures not to the induced secondary fractures.

$$k_f^{'} \times \Delta f = k_f \times w_f \quad (3)$$

Where $k_f^{'} \times \Delta f$ is the product of fracture permeability and width (fracture conductivity), and $k_f \times w_f$ is the corresponding product in the simulation model.

2.4 Model implementation and numeric simulation scheme

A series of numerical models have been conducted to quantitatively determine the influence of various reservoir and completion parameters on performance of MFHW in the process of CO_2 injection(Kalantari-Dahaghi et al., 2015; Liu et al., 2013). These models follow the transport of binary components in a fractured porous shale reservoir pierced by a MFHW. The horizontal well is an injection well located at the center of a circular section that cuts the reservoir vertically as shown in Fig. 1. The numerical simulation model adopts corner-point grid and the simulation area approximates circle. And the pressure of bottom hole is 4MPa higher than the original reservoir pressure.

General, the shale gas reservoir easily realize strongly SRV because of natural fractures and the fragile shale. Therefore, we selected the fracture topology of SRV as the base case, given as Case A1 in Table 2, to figure out the flow regimes of CO_2 injection process. The specific parameters of base case are presented in Table 1. Further, based on the base case, sensitivity studies were conducted to synthetically evaluate the effect of various reservoir and completion parameters on performance of CO_2 injection process. The numerical simulation schemes of sensitivity studies run as follows:

1) In the first set of simulation models, the LGR method is employed to model five kinds of fracture topologies (as shown in Fig.1 and Fig.4). We conduct reservoir numerical simulation to analyze the effect of the fracture topologies on the behavior of CO_2 injection process.

2) Multiply-hydraulic fracturing can easily obtain stimulated reservoir volume(SRV)(Mayerhofer et al., 2008). Based on the topology of SRV, the second set of grids evaluates the effects of primary fractures and secondary fractures (as shown in Fig.1&Fig4.e) on performance of CO_2 injection process. Additionally, we further evaluate the effect of the width of fractured region.

3) The third set examines the effects of various reservoir parameters, including the pressure and permeability of shale reservoir, on performance of multiply-fractured horizontal wells in CO_2 injection process.

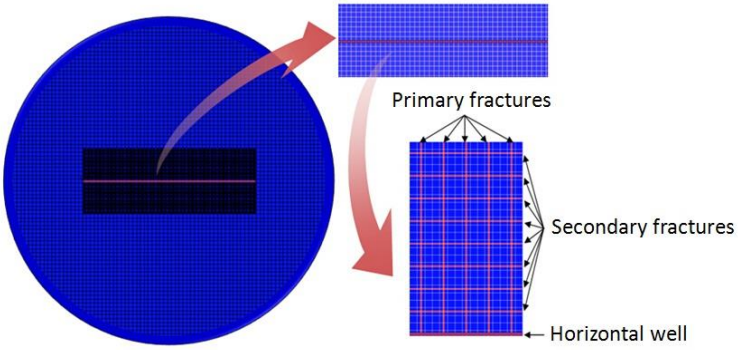

Fig. 1 Top view of SRV fracturing simulation model—Base case

3. Results and analysis

In order to intuitively analyze the effect of various parameters on the performance of CO_2 injection processes, all results are presented in dimensional form. The log-log plot of CO_2 injection rate versus time (LOG-LOG) curve is adopted to identify and illustrate the various flow regimes. This kind of plot can intuitively reveal the different flow regimes and clearly demonstrate the effect of completion and reservoir parameters on the CO_2 injection process.

3.1 Base case results

The Fig.2 presents the LOG-LOG curve obtained from the simulation results of the base case corresponding to case A1 in Table 2. Compared with the result of the triple-porosity model which interprets the flow event of natural gas (100%CH4) in shale reservoir (Al-Ahmadi and Wattenbarger, 2011), the flow regimes are largely consistent. This indicates that the numerical simulation result is reliable. According to the numerical simulation results of the base case A1, eight flow regions can be identified while the CO_2 seepages in the fractured system (as shown in Fig.2-b).

1) Region 1 (IAF): The initial CO_2 adsorption period. During this period, the initial CO_2 injection behaviors are mainly affected by the permeability of hydraulic fractures and the adsorption capability of different component. The CO_2 injection rate remains almost unchanged in a special short time.

2) Region 2 (FLF): The linear flow period in the hydraulic primary fractures, during which the LOG-LOG curve appears with a constant slope (as shown in Fig.2-b). In this period, the gas flow in the reservoirs mainly appears as a linear flow parallel to the surfaces of the hydraulic primary fractures (as shown in Fig.3-a), and hydraulic primary fractures have no effect on each other. Due to the competitive adsorption between CO_2 and CH_4, the LOG-LOG curve did not appear an apparent slope of -1/2 which is obvious in triple-porosity model (as shown in Fig.2-a).

3) Region 3 (FBF): First bilinear flow period, during which the LOG-LOG curve keeps a constant slope of -1/4. During this period, a linear flow occurs in each primary fracture, and the gas flow in the secondary fracture appears as a linear flow perpendicular to the surfaces of the hydraulic primary fractures at the same time (as shown in Fig.3-b). This region corresponds to the region 2 proposed by Al-Ahmadi (as shown in Fig.2-a)(Al-Ahmadi and Wattenbarger, 2011).

4) Region 4 (SLF): The linear flow in the secondary fractures, it will occur once the transient flow in the primary fractures and secondary fractures ends indicating the end of bilinear flow. For the competitive adsorption between CO_2 and CH_4, this flow region also does not exhibit an obvious negative half-slope on the LOG-LOG curve which is different from the region 3 of the triple-porosity model (as shown in Fig.2-a).

5) Region 5 (SBF): The second bilinear flow in both secondary fractures and natural fractures, as shown in Fig.3-c, it is caused by the linear flow in the natural fractures while the secondary fractures are still in transient flow. This flow region exhibits a negative quarter-slope on the LOG-LOG curve, as shown in Fig.3-c, which is similar to the transient flow in region 4 (as shown in Fig.2-a).

6) Region 6 (IBDF): The inner boundary dominated flow. This transient flow regime will only occur when the conductivity ratio between fractured region and shale reservoir is high. The high conductivity ratio will lead to most of the injected CO_2 lagging in fractured region, as shown in Fig.3-d. The CO_2 injection rate will exhibit an exponential decline due to constant bottom-hole pressure and the significant increase of inner fractured region. This flow regime has been proposed by many scholars (Fikri Kuchuk., 2014; Zhou et al., 2012).

7) Region 7 (TLF): The linear flow from fractured region to the un-stimulated shale gas reservoir. However, this transient flow regime only can occur when the length of fractured region is much bigger than the width of that. Most of injected CO_2 will flow to shale gas reservoir perpendicular to the horizontal well, as shown in Fig.3-e. This region exhibits a negative half-slope on the LOG-LOG curve, and it is similar to the region 5(as shown in Fig.2-a). This flow region also has been proposed by Ali (Chen et al., 2015).

8) Region 8 (OBDF): The outer boundary dominated flow, it starts when the pressure transmits to the outer boundary. This flow is governed by exponential decline due to constant bottom-hole pressure, as shown in Fig.3-f.

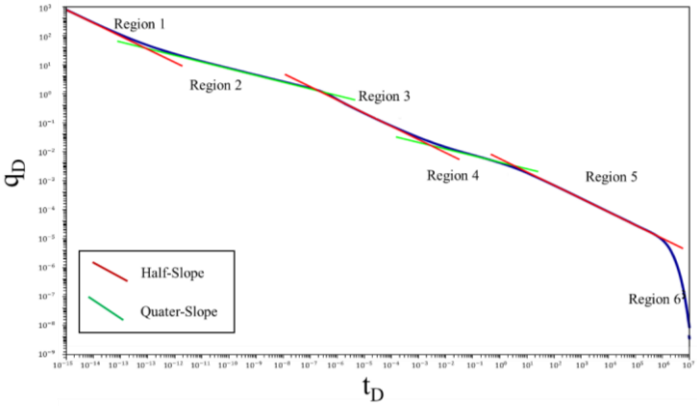

a. The log-log plot of triple-porosity solution (Al-Ahmadi).

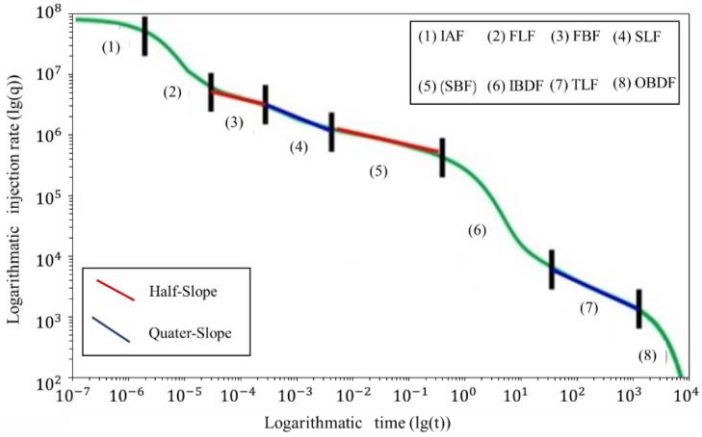

b. The log-log plot of numerical simulation results.

Fig. 2 The comparison between analytical and numerical simulation results

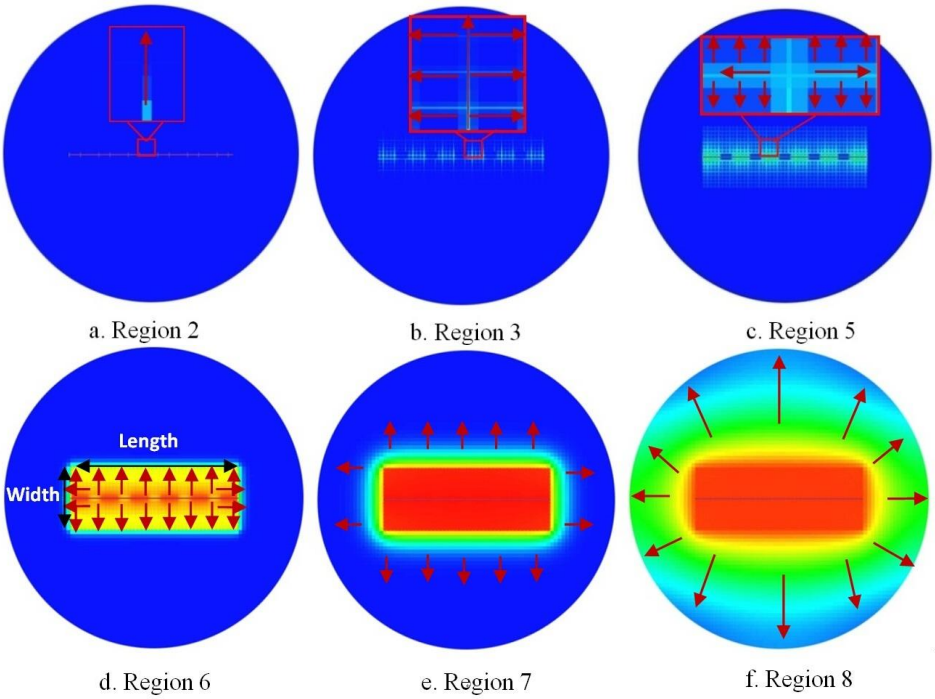

a. Region 2 b. Region 3 c. Region 5

d. Region 6 e. Region 7 f. Region 8

Fig. 3 Flow regimes of a HWFN in numerical simulator—Base case

3.2 Effect of fractured region

3.2 .1 Effect of fracture topology

In order to further analyze the influence of various fracture topologies on performance of MFHW in the process of CO_2 injection, the method of LGR is applied to model the hydraulic fractures to obtain another four kinds of fracture topologies, as shown in Fig.4. The numerical simulation results are shown in Fig.5, and it indicates that fracture topologies mainly affect the flow regimes at early time.

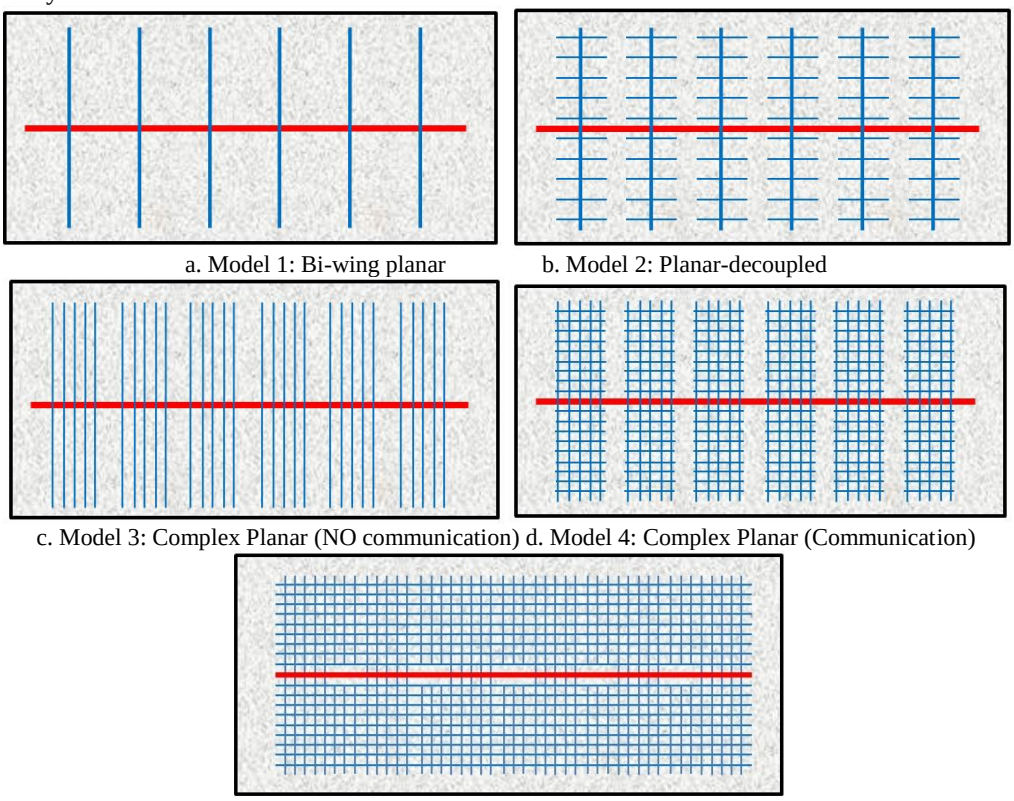

a. Model 1: Bi-wing planar b. Model 2: Planar-decoupled

c. Model 3: Complex Planar (NO communication) d. Model 4: Complex Planar (Communication)

e. Model 5: Network (Base case)

Fig.4 Top view of fracture growth and complexity scenarios

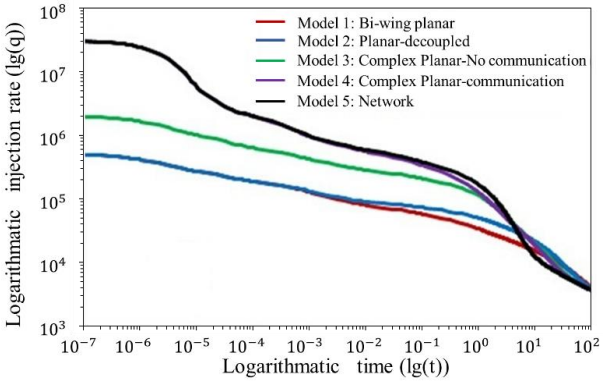

Fig.5 The effect of fracture topologies.

Comparing the LOG-LOG curves of different fracture topologies, the obvious inner boundary dominated region only occur when numerical simulation model is Model 4 or Model 5, as shown in Fig.5, which is notably different from the other three models. For the reason of failing to form complex fracture network (volume fracturing), the other three kinds of fracture topologies can't occur region 4, region 5, and region 6 (as shown in Fig 2-b). We also can figure out that the inner boundary dominated regime reacts more obviously with the increase of stimulated volume. The five LOG-LOG plots will eventually merge in the region 7 at the 100th day (the linear flow from fractured region to shale gas reservoir), such phenomenon indicates that the hydraulic fracturing can only affect the initial CO_2 injection capacity and reservoir physical properties are the main factor controlling injection capacity.

3.2.2 Effect of fracture conductivity

Both natural fractures and fragile shale are unique features of shale reservoirs, and multi-cluster staged hydraulic fracturing can easily create complex fracture network (as shown in Fig.1). Unfortunately, proppant transport cannot be reliably modeled when fracture growth is complex. At present, the distribution of proppant can be classified into three scenarios (Fig.6): 1) If the proppant is confined within a dominant primary fracture (Fig.6-a), this would result in higher conductivity in primary fractures. 2) When the proppant is excessively concentrated in a dominant primary fracture and evenly distributed throughout the secondary fractures (Fig.6-b), the permeability of primary fractures is lower than that of the secondary fractures. 3) Recent studies have illustrated that if the proppant is evenly distributed throughout the whole complex fracture network (Fog.6-c), this would make the permeability of primary fracture equal to that of the secondary fractures. Numerical simulation models were constructed to extensively study the conductivity of propped fractures. In all numerical simulation cases involving primary and secondary fractures, we treat the fracture as possessing a fixed dimensionless conductivity as described in Eq. (4) and Eq. (5) in order to compare the conductivity with values obtained using other models, defined as follows:

$$F_{cd1} = (k_{f1} \times w_{f1}) / (k_f \times x_f) \tag{4}$$

$$F_{cd2} = (k_{f2} \times w_{f2}) / (k_f \times x_f) \tag{5}$$

Where F_{cd} is the dimensionless conductivity between hydraulic fractures and that of natural fractures, k_f is the permeability of the hydraulic fractures, w_f is the width of hydraulic fractures, k_f is the permeability of the natural fractures, and x_f is the width of the natural fractures. Subscripts 1 and 2 respectively represent the primary fractures and the secondary fractures.

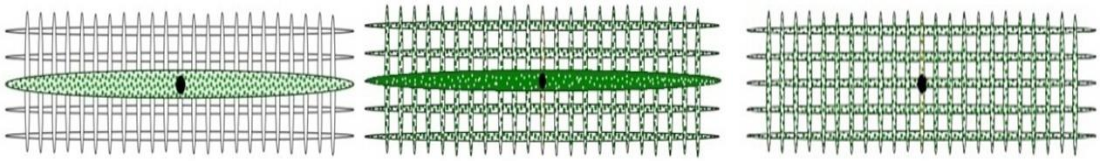

a. Concentrated in a dominanted fracture b. Concentrated &evenly Distributed c. Evenly Distributed

Fig. 6 Proppant transport scenarios-top view (Cipolla et al., 2008)

3.2.2.1 Effect of secondary fractures conductivity

The LOG-LOG curve presented in Figure 7 illustrates the effect of the secondary fracture conductivity on performance of CO_2 injection. The five cases shown in Fig.7 correspond to different secondary fracture conductivities, ranging from a low value of 0.5 to a high value of 100. The sensitivity parameters are given as Cases B1, B2, B3, B4 and B5 in Table 3.

With the increase of the secondary fracture conductivity, the second bilinear regime (Fig.3-c) will be more obvious and the slope of inner boundary dominated flow regime becomes steeper. When the dimensionless conductivity of secondary fractures is 0.5, the second bilinear flow regime will change seriously as shown in Fig.8-a. This pressure map is quite different from that flow regime shown in Fig.3-c. At the same time, the inner boundary dominated flow regime gradually disappears, and the all LOG-LOG curves will finally merge at the linear flow time (from fractured region to shale reservoir), at about 100th day, as shown in Fig.8-b. This illustrates that the variation of secondary fractures conductivity mainly affects the second bilinear and inner boundary dominated flow regimes. Further, we can also find that the other flow regimes almost stay unchanged with the increase of the secondary fractures permeability. This indirectly indicates primary fractures mainly affect the performance of the initial injection flow regime and the physical properties are the principal influence factors in the later injection process.

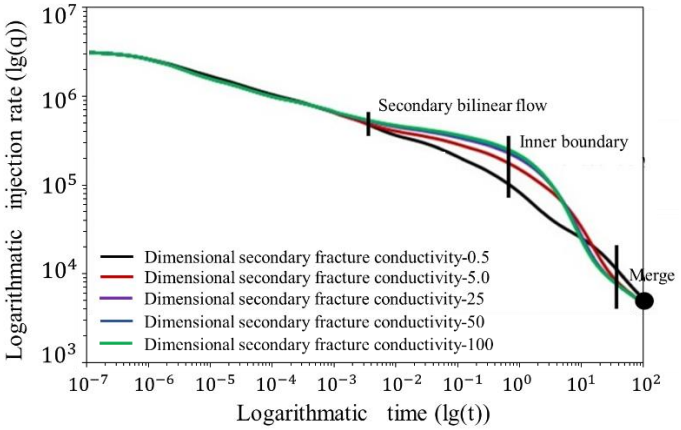

Fig. 7 Varying secondary fracture permeability

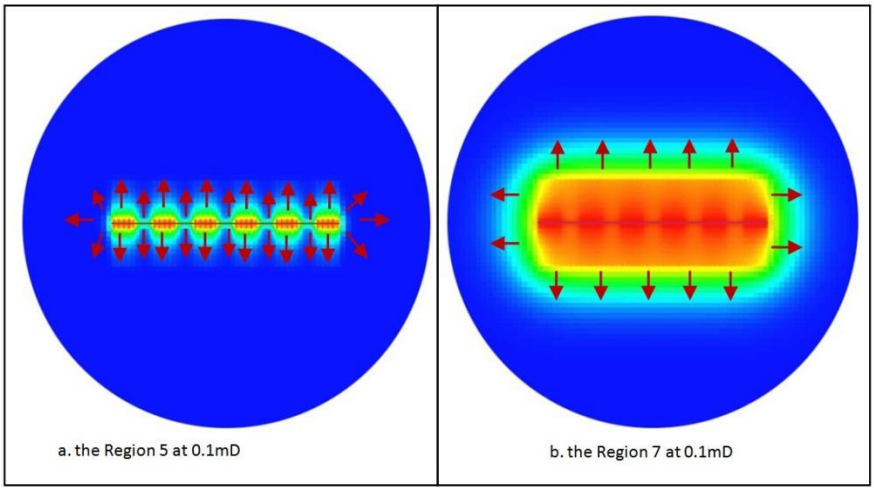

Fig. 8 Varying the conductivity of secondary fracture

3.2.2.2 Effect of primary fractures conductivity

When proppant appears as Fig.6-b shown, the primary fractures permeability will be lower than the secondary fractures permeability. The five cases shown in Fig.9 correspond to different primary fracture conductivities, ranging from a low value of 0.5 to a high value of 100. The sensitivity parameters are given as Cases C1, C2, C3, C4 and C5 in Table 3.

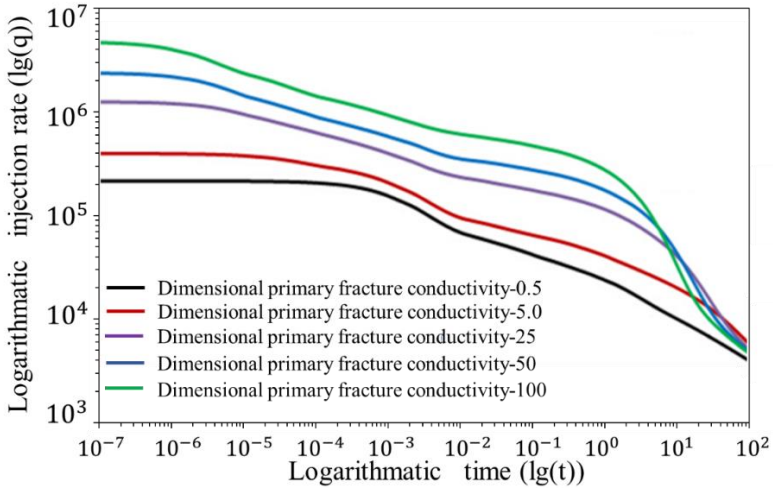

Fig. 9 Varying primary fracture permeability

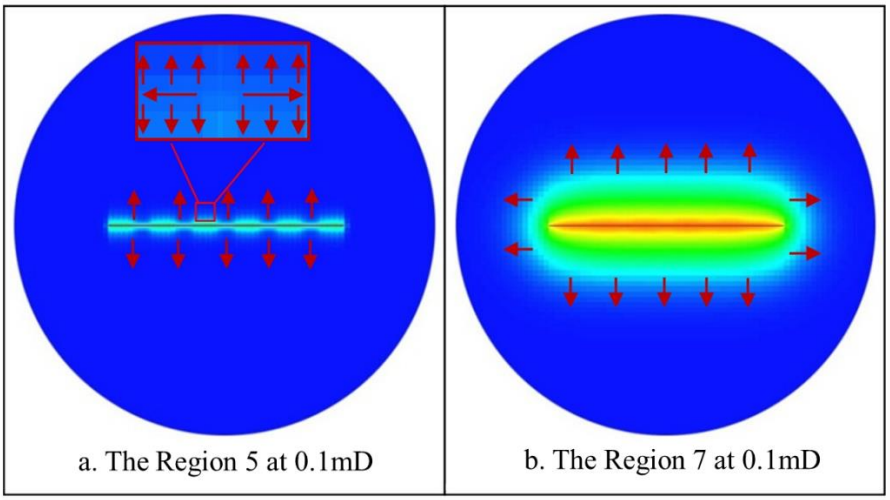

Fig. 10 Varying the conductivity of the primary fracture

Fig.9 and Fig.10 present the effect of the primary fracture conductivity on performance of CO_2 injection. As can be seen, with the decrease of the primary fracture conductivity, the onrushing phenomenon of injected CO_2 along the primary fracture

severely weakens leading to much CO_2 lagging near horizontal well (Fig.10-b). And the time of the initial CO_2 adsorption period obviously extending. Meanwhile, we also find that the linear flow in primary fractures and inner boundary dominated flow fade away with the decrease of the primary fracture conductivity, the second bilinear flow regime (as shown in Fig.9) almost stays unchanged. When the F_{cd1} is 0.5, most initial injected CO_2 would largely lag near the horizontal well. So the second bilinear flow will just happen near horizontal well (as shown in Fig.10-a) which is quite different from that of the base case (as shown in Fig.5-c). All the LOG-LOG curves will finally merge at the linear flow, from fractured region to shale reservoir, for the properties of shale formation.

3.2.2.3 Effect of fracture-network conductivity

When proppant distributes as Fig.6-c shown, the primary fractures permeability is identical with the secondary fractures permeability. The five cases shown in Fig.11 correspond to different hydraulic fracture conductivities, ranging from a low value of 0.5 to a high value of 100. The sensitivity parameters are given as Cases D1, D2, D3, D4 and D5 in Table 3.

Fig.11 presents the effect of the primary hydraulic permeability on performance of CO_2 injection. As can be seen, when the permeability of the primary and secondary fractures decrease at the same time, the variation of the LOG-LOG curves is similar with that of Fig.9. This indicates that the permeability of primary fractures is the major factor controlling the CO_2 injection process.

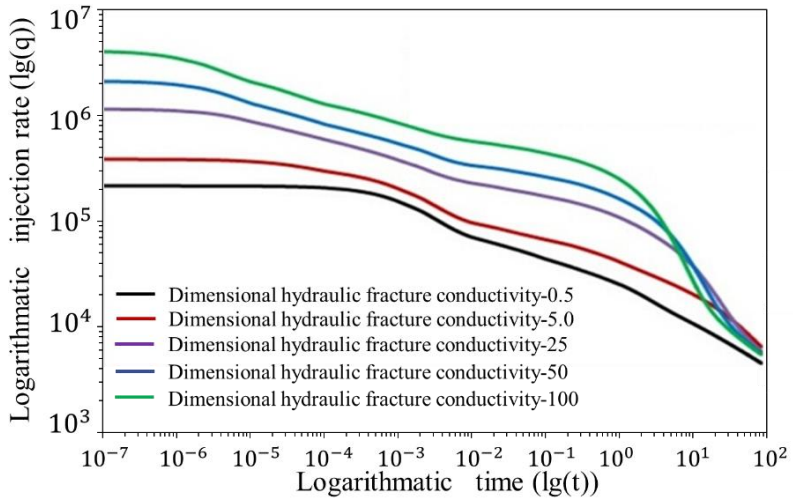

Fig. 11 Varying the permeability of primary and secondary fracture

3.2.3 Effect of SRV size

Fig.12 presents the effect of SRV size on performance of CO_2 injection process. The three cases shown in Fig.12 correspond to different primary fracture conductivities, ranging from a low value of 85m to a high value of 255m. The sensitivity parameters are given as Cases E1, E2, and E3 in Table 4.

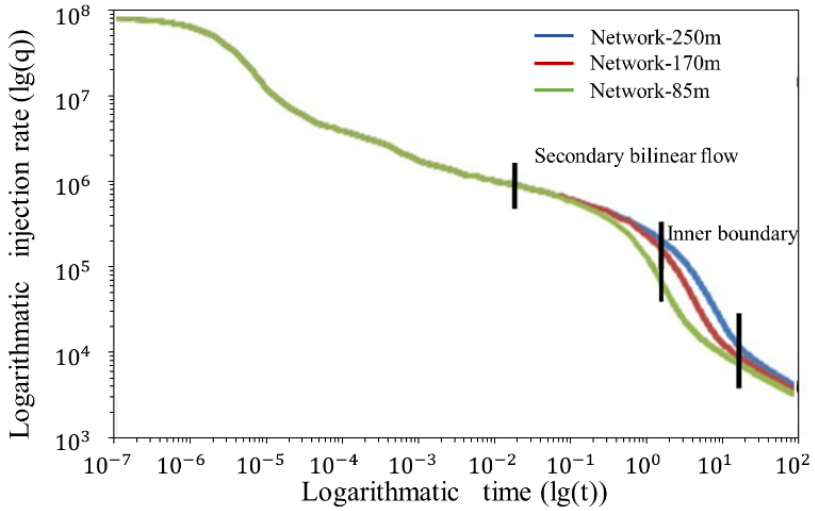

Fig. 12 Varying the width of the fractured region

We can find that the width can only affect the second bilinear and inner boundary dominated flow regimes. With the increase of the fractured region width, the emerging time of the second bilinear flow regime gradually extends and the inner boundary dominated flow regime occurs later. The descending slop of the LOG-LOG curves are identical, which indicates that the width cannot affect the inner boundary dominated flow regime but just postpones the emerging time of inner boundary flow. In general, the width of fractured region has a little influence on the seepage flow process of the CO_2 injection process.

3.3 Effect of reservoir parameters

3.3.1 Effect of permeability of natural fractures

Fig.13 presents the effect of natural fracture permeability on performance of CO_2 injection process. As we can see, the natural fracture permeability can obviously influence the inner boundary dominated flow regime. With the decrease of the dimensionless flow conductivity between hydraulic fracture and natural fracture, the less CO_2 will lag in the fractured region during the inner boundary dominated flow time. This phenomenon makes the inner boundary dominated flow regime fade away, and it manifests as the slop of the LOG-LOG curve gradually decreases. All the LOG-LOG curves can't merge, which further indicates that the reservoir parameter is the main factor affecting the flow event of CO_2.

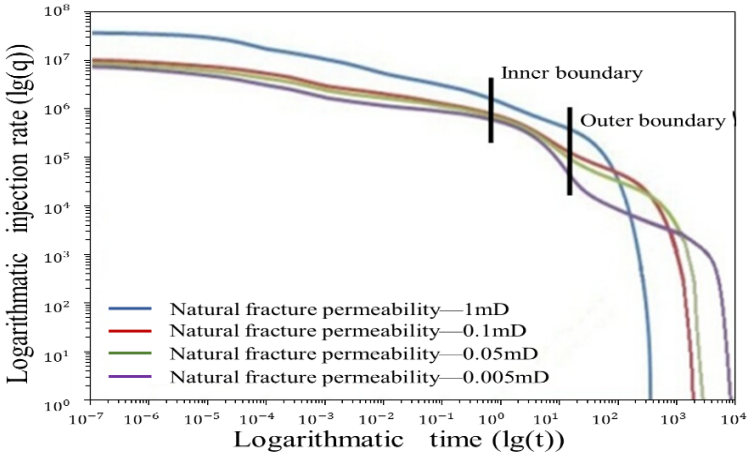

Fig. 13 Varying the permeability of natural fractures

3.3.2 Effect of reservoir pressure

Fig.14 describes the effect of reservoir pressure on performance of CO_2 injection process. By comparison with the type curves getting from the base case, the reservoir pressure has little effect on the performance on the CO_2 injection process. With the reservoir pressure decreasing, the compression properties of CO_2 and CH_4 gradually enhance and the early CO_2 injection rate gradually decreases. And the flow regimes after the inner boundary dominated regime occur later. Finally, all the LOG-LOG curves will merge at the 100th day, which indicates that the main control factor is not reservoir pressure but the reservoir permeability.

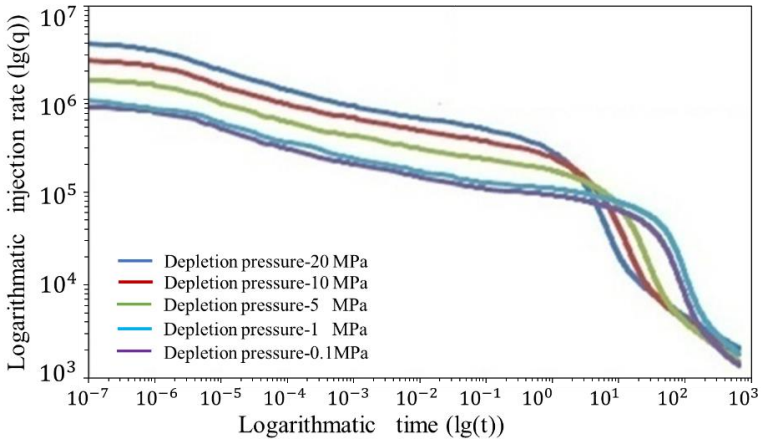

Fig. 14 varying the reservoir pressure

4. Conclusion

To characterize the influence of various reservoir and completion parameters on CO_2 injection process in shale gas systems, this work employs numerical method to analyze the pressure performance of MFHW. Local grid refinement method is applied to model complex fracture networks. After series of numerical simulation studies, we draw some meaningful conclusions:

- Simulation results of base case illustrate that eight flow regimes can be identified: (1) IAF. (2) FLF. (3) FBF. (4) SLF. (5) SBF. (6) IBDF (7) TLF. (8) OBDF. The occurrence of IBDF and OBDF is related to permeability contrast between fracture networks and shale reservoir.
- Fracture geometries with complex fracture network have three unique flow regimes: (1) SLF; (2) SBF (3) IBDF. The occurrence of these three flow regimes is related to forming a huge stimulated reservoir volume.
- Flow regimes affected by permeability of secondary fractures are SBF and IBDF. As the conductivity of secondary fracture increases, the SBF will extend longer and the IBDF occurs later.
- Flow regimes affected by conductivity of primary fractures are FLF, FBF, IBDF, and SBF. As the conductivity of primary fracture decreases, the FLF, FBF, and IBDF gradually disappear and the SBF hardly changes.
- Reservoir parameters can dominate the IBDF. Decreasing the permeability of natural fractures, the IBDF will extend longer. Moreover, the effect of reservoir pressure on the pressure performance is little.

This work employs numerical method for synthetically forecasting the pressure performance of MFHW in CO_2 injection process. Given that complex fracture networks and complex CO_2 adsorption phenomenon exist in real cases, the numerical approach can not accurately simulate all cases. However, this work can enlarge our knowledge of CO2 injection in shale gas systems.

Nomenclatures

A	empirical correction factor for D
D	diffusion and dispersion coefficient
k	permeability
N	the moles per unit of grid block
P	pressure
P_L	Langmuir pressure
t	time
T	transmissibility factor
V	gird block volume
V_{ads}	the potential releasable-gas content
w	the width of fracture
y	the mole fraction in gas phase
ρ	molar concentration
$\emptyset$	porosity

Acknowledgement

We are grateful to any reviewers for their insightful and constructive comments for improving the manuscript. This work was funded by National Basic Research 973 Program of China (2015CB250900) and The Important Project of science and technology in developing great oil&gas field and coal bed gas (2016ZX05047-004).

References:

Al-Ahmadi, H.A. and Wattenbarger, R.A., 2011. Triple-porosity Models: One Further Step Towards Capturing Fractured Reservoirs Heterogeneity. Presented at the SPE/DGS Saudi Arabia Section Technical Symposium and Exhibition, 15-18 May, Al-Khobar, Saudi Arabia.

Ali, A.J., Siddiqui, S. and Dehghanpour, H., 2013. Analyzing the production data of fractured horizontal wells by a linear triple porosity model: Development of analysis equations. Journal of Petroleum Science and Engineering, 112: 117-128.

Bacon, D.H., Yonkofski, C.M.R., Schaef, H.T., White, M.D. and McGrail, B.P., 2015. CO2 storage by sorption on organic matter and clay in gas shale. Journal of Unconventional Oil and Gas Resources, 12: 123-133.

Brown, M., Ozkan, E., Raghavan, R. and Kazemi, H., 2011. Practical Solutions for Pressure-Transient Responses of Fractured Horizontal Wells in Unconventional Shale Reservoirs. SPE Reservoir Evaluation & Engineering, 14(06): 663 - 676.

Bumb, A.C. and Mckee, C.R., 1988. Gas-Well Testing in the Presence of Desorption for Coalbed Methane and Devonian Shale. Spe Formation Evaluation, 3(1): 179-185.

Chen, Z., Liao, X., Zhao, X., Dou, X. and Zhu, L., 2015. Performance of horizontal wells with fracture networks in shale gas formation. Journal of Petroleum Science and Engineering, 133: 646-664.

Cipolla, C.L., Warpinski, N.R., Mayerhofer, M.J., Lolon, E. and Vincent, M.C., 2008. The Relationship Between Fracture Complexity, Reservoir Properties, and Fracture Treatment Design. Presented at the SPE Annual Technical Conference and Exhibition, 21-24 September, Denver, Colorado, USA. SPE-115769-MS.

Dongyan, F., Jun, Y., Hai, S., Hui, Z. and Wei, W., 2015. A composite model of hydraulic fractured horizontal well with stimulated reservoir volume in tight oil & gas reservoir. Journal of Natural Gas Science and Engineering, 24: 115-123.

Eshkalak, M.O., Al-Shalabi, E.W., Sanaei, A., Aybar, U. and Sepehrnoori, K., 2014a. Simulation study on the CO2-driven enhanced gas recovery with sequestration versus the re-fracturing treatment of horizontal wells in the U.S. unconventional shale reservoirs. Journal of Natural Gas Science and Engineering, 21: 1015-1024.

Eshkalak, M.O., Al-Shalabi, E.W., Sanaei, A., Aybar, U. and Sepehrnoori, K., 2014b. Simulation study on the CO2-driven enhanced gas recovery with sequestration versus the re-fracturing treatment of horizontal wells in the U.S. unconventional shale reservoirs. Journal of Natural Gas Science and Engineering, 21: 1015-1024.

Fikri Kuchuk., D.B., 2014. Pressure-Transient Behavior of Continuously and Discretely Fractured Reservoirs.

Freeman, C.M., Moridis, G., Ilk, D. and Blasingame, T.A., 2013. A numerical study of performance for tight gas and shale gas reservoir systems. Journal of Petroleum Science and Engineering, 108: 22-39.

Godec, M., Koperna, G., Petrusak, R. and Oudinot, A., 2013. Potential for enhanced gas recovery and CO2 storage in the Marcellus Shale in the Eastern United States. International Journal of Coal Geology, 118: 95-104.

Jones, J.R., Volz, R. and Djasmari, W., 2013. Fracture Complexity Impacts on Pressure Transient Responses From Horizontal Wells Completed With Multiple Hydraulic Fracture Stages.

Kalantari-Dahaghi, A., Mohaghegh, S. and Esmaili, S., 2015. Data-driven proxy at hydraulic fracture cluster level: A technique for efficient CO2- enhanced gas recovery and storage assessment in shale reservoir. Journal of Natural Gas Science and Engineering, 27: 515-530.

Liu, F., Ellett, K., Xiao, Y. and Rupp, J.A., 2013. Assessing the feasibility of CO2 storage in the New Albany Shale (Devonian–Mississippian) with potential enhanced gas recovery using reservoir simulation. International Journal of Greenhouse Gas Control, 17: 111-126.

Liu, M. et al., 2015. Sensitivity analysis of geometry for multi-stage fractured horizontal wells with consideration of finite-conductivity fractures in shale gas reservoirs. Journal of Natural Gas Science & Engineering, 22: 182-195.

Mayerhofer, M.J., Lolon, E., Warpinski, N.R. and Cipolla, C.L., 2008. What is Stimulated Reservoir Volume (SRV). Presented at the SPE Shale Gas Production Conference, 16-18 November, Fort Worth, Texas, USA.

Ren, J. and Guo, P., 2015. A novel semi-analytical model for finite-conductivity multiple fractured horizontal wells in shale gas reservoirs. Journal of Natural Gas Science & Engineering, 24: 35-51.

Ritter, J.A. and Yang, R.T., 1987a. Equilibrium adsorption of multicomponent gas mixtures at elevated pressures. Industrial & Engineering Chemistry Research, 26(8): 1679-1686.

Ritter, J.A. and Yang, R.T., 1987b. Equilibrium adsorption of multicomponent gas mixtures at elevated pressures. Industrial & Engineering Chemistry Research, 26(8): 1679-1686.

Ruthven, D.M., 1984. Principles of adsorption and adsorption processes. Wiley, 168-179 pp.

Schettler, P.D. and Parmely, C.R., 1991. Contributions to Total Storage Capacity in Devonian Shales. Paper SPE-23422-MS presented at the SPE Eastern Regional Meeting, Lexington, Kentucky，22-25 October.

Stalgorova, E.M.L., 2012. Practical Analytical Model to Simulate Pro duction of Horizontal Wells with Branch Fractures.

Stalgorova, K. and Mattar, L., 2013. Analytical Model for Unconventional Multifractured Composite Systems. SPE Reservoir Evaluation & Engineering, 16(03): 246-256.

Stehfest, H., 1970. Algorithms 368： Numerical Inversion of Laplace Transforms. Commun. of the ACM, 13(1): 47-49.

Sureshjani, M.H. and Clarkson, C.R., 2015. Transient linear flow analysis of constant-pressure wells with finite conductivity hydraulic fractures in tight/shale reservoirs. Journal of Petroleum Science & Engineering, 133(3): 455-466.

Wang, H.T., 2014. Performance of multiple fractured horizontal wells in shale gas reservoirs with consideration of multiple

mechanisms. Journal of Hydrology, 510(3): 299-312.
Yu, W., Al-Shalabi, E.W. and Sepehrnoori, K., 2014. A Sensitivity Study of Potential CO2 Injection for Enhanced Gas Recovery in Barnett Shale Reservoirs. Paper SPE-169012-MS presented at the SPE Unconventional Resources Conference, The Woodlands, Texas, USA, 1-3 April.
Zhou, W., Banerjee, R., Poe, B.D., Spath, J. and Thambynayagam, M., 2012. Semi-Analytical Production Simulation of Complex Hydraulic Fracture Network.

Appendices

Table 1 Average parameters of Barnet shale in Case A1 from Table 2.

Types	Parameters	Value	Unit	Source
Reservoir	Grid spacing	20*20*2.0	m	\
	Circular model diameter	1620	m	(Heller and Zoback, 2014)
	Reservoir thickness	10	m	\
	Porosity of matrix	2	%	(Heller and Zoback, 2014)
	Porosity of fracture	0.1	%	(Heller and Zoback, 2014)
	Natural fracture permeability	0.01	mD	(Heller and Zoback, 2014)
	k_v/k_h	0.1	\	(Heller and Zoback, 2014)
	Initial reservoir pressure, P_i	24	Mpa	(Heller and Zoback, 2014)
	Density of rock,	2500	kgm^{-3}	(Heller and Zoback, 2014)
	Reservoir temperature	115	℃	(Heller and Zoback, 2014)
Shale gas	Langmuir volume of CH_4	40	atm	(Heller and Zoback, 2014)
	Langmuir pressure of CH_4	2.1	cm^3/g	(Heller and Zoback, 2014)
	Langmuir volume of CO_2	32.8	atm	(Heller and Zoback, 2014)
	Langmuir pressure of CO_2	4.2	cm^3/g	(Heller and Zoback, 2014)
Fractured well	Horizontal well length, L_H	1000	m	(Heller and Zoback, 2014)
	Fracture half-length	170	m	(Heller and Zoback, 2014)
	Primary fracture permeability, K_{pf}	30	mD	(Heller and Zoback, 2014)
	Secondary fracture permeability, K_{sf}	30	mD	(Heller and Zoback, 2014)
	Injection bottom-hole pressure	28	MPa	\

Table 2 Description of the simulation runs and sensitivity analyses varying fracture topologies.

Case	Permeability		Fracture topology
	Hydraulic fractures/mD	Natural fracture/mD	
A1	30	0.01	Base case
A2	30	0.01	Model 1
A3	30	0.01	Model 2
A4	30	0.01	Model3
A5	30	0.01	Model 4

Table 3 Description of the simulation runs and sensitivity analyses varying fracture conductivity.

Case	Permeability					Fracture topology
	Primary fracture/mD	Secondary fracture/mD	Natural fracture/mD	F_{cd1}	F_{cd2}	
B1	30	0.1	0.01	150	0.5	Base case
B2	30	1	0.01	150	5.0	Base case
B3	30	5	0.01	150	25	Base case
B4	30	10	0.01	150	50	Base case
B5	30	20	0.01	150	100	Base case
C1	0.1	30	0.01	0.5	150	Base case
C2	1	30	0.01	5.0	150	Base case
C3	5	30	0.01	25	150	Base case
C4	10	30	0.01	50	150	Base case
C5	20	30	0.01	100	150	Base case
D1	0.1	0.1	0.01	0.5	0.5	Base case
D2	1	1	0.01	5.0	5.0	Base case
D3	5	5	0.01	25	25	Base case
D4	10	10	0.01	50	50	Base case
D5	20	20	0.01	100	100	Base case

Table 4 Description of the simulation runs and sensitivity analyses varying fractured region width and reservoir parameters.

Case	Permeability			Reservoir pressure/MPa	Fractured region width/m	Fracture topology
	Hydraulic fractures/mD	Natural fracture/mD	F_{cd1}= F_{cd2}			
E1	30	0.01	150	22	85	Base case
E2	30	0.01	150	22	170	Base case
E3	30	0.01	150	22	255	Base case
F1	30	0.005	300	22	170	Base case
F2	30	0.05	30	22	170	Base case
F3	30	0.1	3.0	22	170	Base case
G1	30	1	0.3	22	170	Base case
G2	30	0.01	150	20	170	Base case
G3	30	0.01	150	10	170	Base case
H1	30	0.01	150	5	170	Base case
H2	30	0.01	150	1	170	Base case
H3	30	0.01	150	0.1	170	Base case